



Nonlinear optical property and application of yttrium oxide in erbium-doped fiber lasers

WENJUN LIU,^{1,2}  TUO SHI,³ MENGLI LIU,¹ QIAN WANG,¹ XIMEI LIU,¹ QIN ZHOU,^{4,5,6} MING LEI,¹ PENGFEI LU,^{1,5,7} LI YU,¹ AND ZHIYI WEI^{2,5,8} 

¹State Key Laboratory of Information Photonics and Optical Communications, School of Science, Beijing University of Posts and Telecommunications, P. O. Box 91, Beijing 100876, China

²Beijing National Laboratory for Condensed Matter Physics, Institute of Physics, Chinese Academy of Sciences, Beijing 100190, China

³Institute of Microelectronics of Chinese Academy of Sciences, Beijing 100029, China

⁴School of Electronics and Information Engineering, Wuhan Donghu University, Wuhan 430212, China

⁵These authors contributed equally.

⁶qinzhou@whu.edu.cn

⁷photon.bupt@gmail.com

⁸zywei@iphy.ac.cn

Abstract: Yttrium oxide (Y_2O_3) has garnered some attention in view of its potential to be integrated into a wide range of high-strength structural components, microelectronic and optoelectronic devices. However, the nonlinear optical research of this promising material has not been implemented yet. In this paper, not only the electronic band structures of Y_2O_3 are theoretically calculated but also the optical nonlinearity of Y_2O_3 is validated by using the fiber laser as a platform. Meanwhile, the influence of sample thickness on laser performance is further explored by using Y_2O_3 saturable absorbers with different thickness. Results indicate that Y_2O_3 not only has impressive optical nonlinearity but also is beneficial to the investigation of ultrafast photons by adjusting the thickness of Y_2O_3 . Therefore, Y_2O_3 can be used as a potential saturable absorber candidate for in-depth research and application.

© 2021 Optical Society of America under the terms of the [OSA Open Access Publishing Agreement](#)

1. Introduction

Since the application of graphene in electronics and optoelectronics [1,2], more and more two-dimensional (2D) materials have coming into our vision. In addition to the widely studied 2D materials including transition metal dichalcogenides (TMDs) [3–5], topological insulators (TIs) [6,7] and black phosphorus (BPs) [8], some emerging materials, such as MXene and black phosphorus quantum dots [9,10], have also attracted considerable attention because of their differentiation advantages. However, attempts and explorations to find promising materials that perform better have never stopped.

In recent years, yttrium oxide (Y_2O_3) has garnered the attention in view of its potential to be integrated into a wide range of high-strength structural components, microelectronic and optoelectronic devices [11–13]. Y_2O_3 is a cubic structure rare-earth oxide. The melting point of Y_2O_3 is about 2439°C, which enables it to have special physical properties and high crystal stability [14,15]. Meanwhile, the dielectric constant of Y_2O_3 is measured up to 15, which indicates that it can be used as an excellent dielectric material [16]. It is worth mentioning that the Y_2O_3 shows low lattice-mismatch with Si, as a result, it is generally considered to be a substitute for SiO_2 in complementary metal oxide semiconductor (CMOS) devices [17]. As a rare earth oxide, Y_2O_3 is a research hotspot of potential waveguide lasers. Meanwhile, the large refractive index of Y_2O_3 enable it to be an excellent waveguide material, allowing integrated waveguide lasers to have lower thresholds and outstanding thermal management [18]. Although

Y_2O_3 has impressive photoelectric properties and can be used in Q-switched laser as saturable absorbers (SAs) [19], the application of Y_2O_3 in the mode-locked laser has not been reported.

For traditional 2D material SAs, there are some commonly used fabrication methods such as mechanical exfoliation, magnetron sputtering, chemical vapor deposition, etc [20–23]. In the production of Y_2O_3 , the magnetron sputtering method is applicable, and has the advantages of simple operation and low cost. Meanwhile, in order to enhance the nonlinearity of SA, the microfiber structure is chosen. The two major influencing factors, waist diameter and length of fused zone, are carefully chosen and controlled.

In this paper, the electronic band structures of Y_2O_3 are theoretically calculated, and the possible application of Y_2O_3 in nonlinear optics is verified. Fiber lasers with great system robustness, high beam quality is used as ideal platforms for exploring the optical nonlinearity of materials. Although passively Q-switched fiber laser with Y_2O_3 has been realized [19], the mode-locking phenomenon requires the balance of the dispersion and nonlinearity, and the conditions are more stringent. Here, the passively mode-locked fiber lasers (PMLFL) based on Y_2O_3 are realized after employing Y_2O_3 as the SA into the laser cavity. Besides, the influence of sample thickness on laser performance is further explored. Results indicates that Y_2O_3 not only has good optical nonlinearity, but also is beneficial to the investigation of ultrafast photons by adjusting the thickness of Y_2O_3 .

2. Results

2.1. Characteristics

The Y_2O_3 SA with microfiber structure is manufactured by means of magnetron sputtering deposition method. Initially, the Y_2O_3 raw material with a purity of 99.99% is prepared. Meanwhile, the microfibers with evanescent field interaction of 12 μm and fused zone of 5 mm are in place. Choosing the micro-fiber with small waist diameter and long fused zone is able to enhance the nonlinearity of SA and facilitate the establishment of the mode-locking system. After loading the Y_2O_3 target and fixing the microfiber, the vacuum of sputtering chamber is pumped to 1×10^{-3} Pa. During the deposition, sputtering power is set as 80 W, and the flow rates of Ar and O_2 are maintained at 20 and 0.2 sccm, respectively. By controlling sputtering time, three kinds of Y_2O_3 SA with different thickness are obtained. Finally, Y_2O_3 wrap around the evanescent field zone of the tapered fiber.

The chemical composition of the prepared Y_2O_3 are characterized by the X-ray photoelectron spectroscopy (XPS). In the O-1s XPS spectra of Y_2O_3 (Fig. 1(A)), the main peak is decomposed into three peaks, which locate at 531 eV, 531.9 eV and 533.07 eV. The peak at 531 eV is the contribution from O-Y bond. The peaks at 531.9 eV and 533.07 eV show the existence of Y-O-Si and O-Si bonds, which may come from the diffusion of the substrate silicon. Similarly, in the XPS spectra of Y-3d (Fig. 1(B)), the two peaks located at 158.37 eV and 160.32 eV are assigned to the contribution of Y $3d_{5/2}$ state and the Y $3d_{3/2}$ state. The XPS spectra of Y_2O_3 are in good agreement with previous results [24]. The absorption spectrum indicates that the absorptivity of Y_2O_3 to light is 38.416% at 1550 nm (Fig. 1(C)).

To achieve the nano-scale observation and measurement of three prepared Y_2O_3 film, the high-resolution atomic force microscopy (AFM) is employed. The surface topography and thickness measurements of three different Y_2O_3 film are shown in Figs. 1(D)–1(I). On the whole, the surfaces of the three samples are uniform. The thinnest of the Y_2O_3 sample owns a thickness of 5 nm through testing the sample on the silicon wafer while preparing the sample on the tapered fiber (Fig. 1(G)). Due to the coating thickness is positively related to the coating time, the tapered fiber has the same thickness Y_2O_3 as the wafer on the planar silicon. Similarly, the thicknesses of the other two materials are measured as 8 nm and 20 nm (Figs. 1(H) and 1(I)). Optical nonlinearity as an important characteristic of the Y_2O_3 SA is measured by the double balance detection method. The pump source used in the measurement is homemade. The corresponding operation

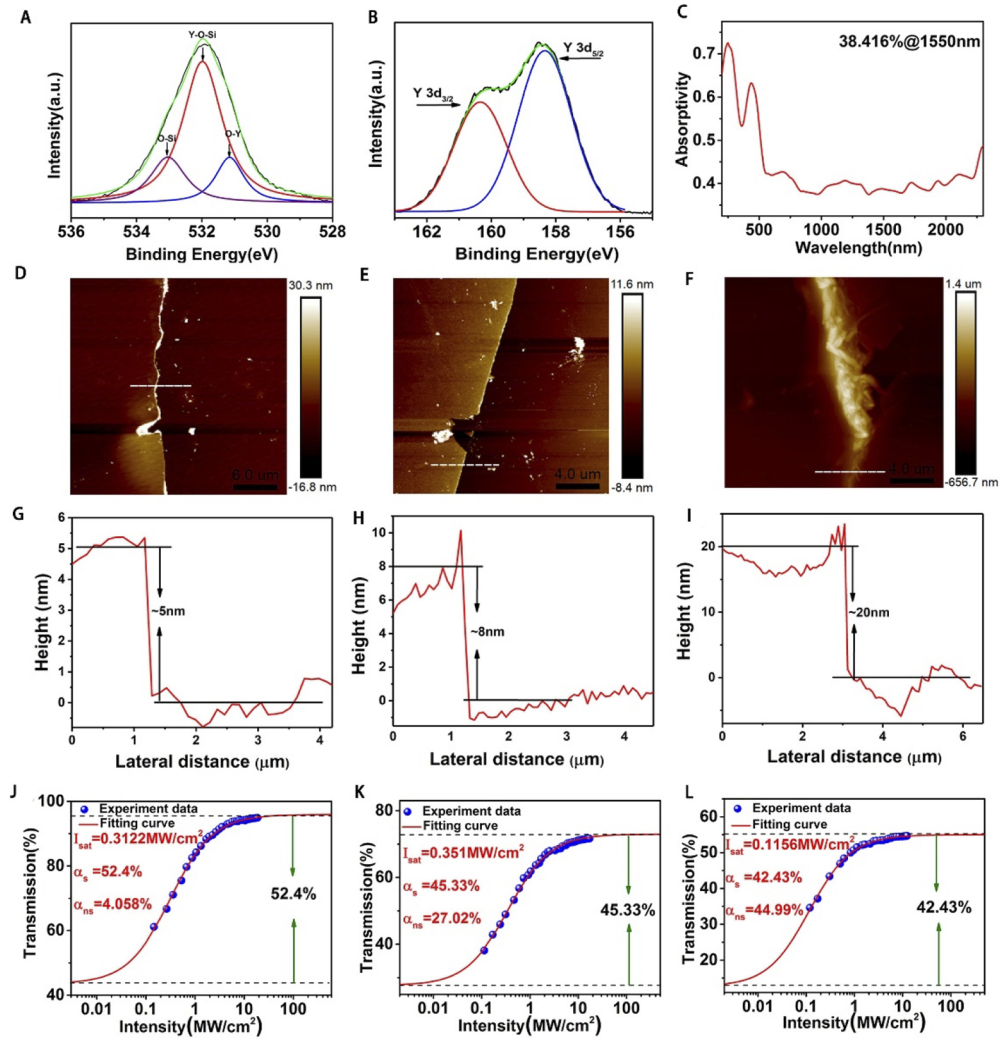


Fig. 1. The characterization of Y_2O_3 . (A) The O-1s spectra of Y_2O_3 . (B) The Y-3d spectra of Y_2O_3 . (C) The absorption spectrum of Y_2O_3 films. The AFM of (D)(G) 5-nm, (E)(H) 8-nm and (F)(I) 20-nm Y_2O_3 films. The nonlinear absorption of (J) 5-nm- (K) 8-nm- (L) 20-nm- Y_2O_3 films.

bandwidth, repetition frequency and pulse duration of mentioned mode-locked laser are 1550 nm, 120 MHz, and 700 fs, respectively. After the measurement, the optical nonlinearity curves of three samples varying with input power are plotted (Figs. 1(J)–1(L)). The modulation depth (MD) and saturated absorption intensity (I_{sat}) of 5-nm Y_2O_3 SA are 52.4% and 0.3122 MW/cm^2 (Fig. 1(J)). The MD of 8-nm and 20-nm Y_2O_3 SA are fitted as 45.33% and 42.43% (Figs. 1(K) and 1(L)). The modulation depth is related to the relaxation time. When the number of layers of the material increases, the direct band gap becomes an indirect band gap, which increases the difficulty of free electron migration. The carrier relaxation time becomes lower, and the modulation depth decreases [25]. The insertion loss of the SAs are 2.15 dB (5 nm), 4.2 dB (8 nm), 4.6 dB (20 nm), respectively.

2.2. Band structure and total energy calculations

The band structures of Y_2O_3 films are investigated by the first-principles calculations. By using the plane-wave technique in Vienna ab initio simulation package (VASP), the first-principles theory calculations are completed [26–28]. The plane waves are expanded with an energy cut of 520 eV. The convergence criterion for total energy was 10^{-4} eV. All the atomic positions and lattice structures were fully relaxed with the threshold of 0.01 eV/Å. Monkhorst-Pack scheme is used to performed $1\times 1\times 1$ and $15\times 15\times 15$ k-point mesh for the bulk and few-layer models in the Brillouin Zone integration, respectively [29]. A vacuum layer of 15 Å is built to avoid periodic interactions. Hey-Scuseria-Ernzerhof hybrid functional (HSE06) was employed for the electronic structure calculation of Y_2O_3 monolayer [30,31].

Y_2O_3 bulk is a body-centered cubic lattice system with space group (No.206), which is similar to Ho_2O_3 and Dy_2O_3 . It has a lattice parameter of 10.7 Å with 80 atoms in the unit cell (Fig. 2(A)). Each Y atom is six-fold coordinated to oxygen atoms, and each O atom is surrounded by four Y atoms in the form of a distorted tetrahedron. According to previous studies, Y_2O_3 is an excellent insulator with a wide energy band gap of 6 eV [32,33]. Here we model the clean Y_2O_3 (111) plane for the investigation of Y_2O_3 films. After full relaxation, the Y_2O_3 (111) monolayer forms a nearly planar structure with a lattice constant of 7.18 Å (Figs. 2(B)–2(D)). The band structure of Y_2O_3 (111) monolayer notes that Y_2O_3 monolayer is a direct band gap semiconductor with both conduction band minimum (CBM) and the valence band minimum (VBM) located at the Γ point, and the obtained band gaps are 2.55 eV and 3.93 eV for GGA-PBE and HSE06 level (Fig. 2(C)), respectively. These results are in good agreement with the previous reports, however, the band gap of Y_2O_3 monolayer is much smaller than that of the bulk one, which is due to the different bond characters [34].

The prepared Y_2O_3 films have an absorptivity of 38.416% at 1550 nm, corresponding to a possible band gap less than 0.8 eV, which is smaller than the gap of Y_2O_3 monolayer. It is generally believed that light absorptivity is greatly associated with the structural defects in samples, which are mainly introduced during the growth process. Previous studies have reported there is the high density of preexisting defects in the deposited Y_2O_3 films on silicon substrates, and the major defects are oxygen vacancies [35]. In our experiment, the thicknesses of three prepared Y_2O_3 samples are 5 nm, 8 nm, and 20 nm, respectively. Thus, a 3-layer Y_2O_3 model containing 6 Y atoms and 9 O atoms was constructed for the calculation of defect structure with a reasonable balance of computation cost. Without oxygen vacancies, the 3-layer Y_2O_3 film performs a direct band gap of 2.09 eV at the PBE level (Fig. 2(E)). By removing one oxygen atom in 3-layer Y_2O_3 film, the system remains a planar structure and the band gap can be decreased by about 1 eV. By comparing the obtained band structure (Figs. 2(F)–2(I)), we can find that the position of the oxygen vacancy defect has little impact on the electronic structure. In the case of two oxygen atom missing, the optimized structure performs a low-buckled geometry, and the band gap is decreased to 0.37 eV. Thus, we can conclude that the existence of oxygen vacancies can induce the reduction of the band gap in the system of Y_2O_3 film, and it could be the reason for the absorption of Y_2O_3 films to light at 1550 nm.

2.3. Mode-locked fiber laser

The design diagram of laser used is the loop cavity (Fig. 3(A)). Considering the merits of alignment-free operation, great system robustness, high beam quality and pumping efficiency, the fiber laser is deemed to be an ideal platform for the confirmation of the optical nonlinearity of Y_2O_3 . At the same time, by maintaining the laser cavity device, the influence of sample thickness on the laser performance can be further studied. Here, PMLFL is constructed to investigate the saturable absorption characteristics of three Y_2O_3 SAs with different thickness. As the gain medium, a 0.4-m erbium-doped fiber (EDF, Liekki 110 –4/125) owns the absorption coefficient of 250 dB/m at 980 nm. The total cavity length is 2.5 m, including 0.4 m EDF (-17.193

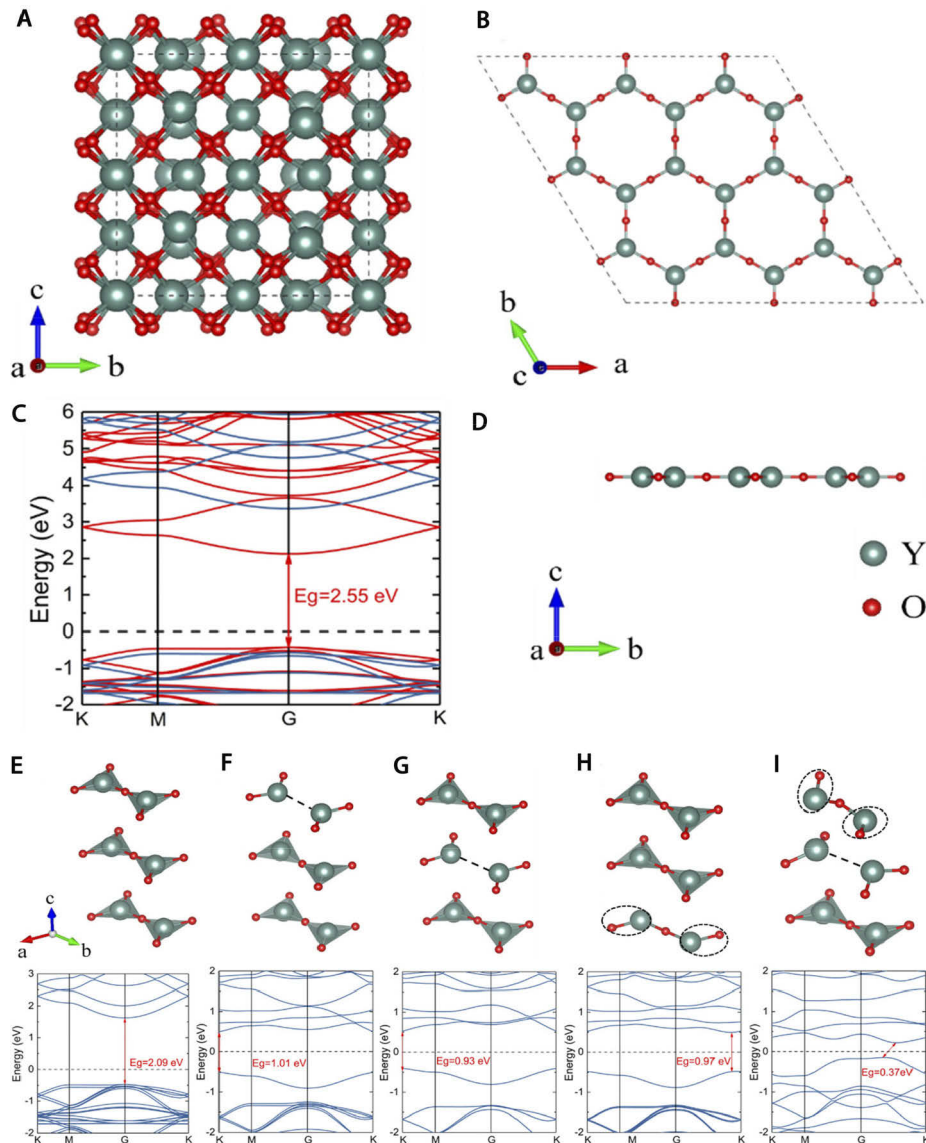


Fig. 2. The atomic structure and band structure of Y_2O_3 . (A) Atomic structure of bulk Y_2O_3 . (B) Top views of Y_2O_3 monolayer. (C) Calculated band structure of monolayer Y_2O_3 by using GGA-PBE (red thick lines) and HSE06 (blue thin lines) approaches. (D) Side views of monolayer. Yttrium and oxygen atoms are shown in green and red, respectively. (E) Optimized geometries of 3-layer Y_2O_3 films without vacancy defect. (F) Single oxygen vacancy at the top layer. (G) Single oxygen vacancy at the medium layer. (H) Single oxygen vacancy at the bottom layer. (I) Two oxygen vacancies in 3-layer Y_2O_3 films. The band structures of these models are shown below the corresponding structure. The Fermi level is set to be 0 eV and indicated by the black dash line.

$\text{ps}\cdot\text{nm}^{-1}\cdot\text{km}^{-1}$) and 2.1 m single mode fiber (SMF, $17.002 \text{ ps}\cdot\text{nm}^{-1}\cdot\text{km}^{-1}$), the total dispersion is -0.376 ps^2 . To achieve a balance between dispersion and nonlinearity, the 2.5 m cavity length, 12 μm waist diameter and 0.7 cm fusion zone length of the laser is used, which is different with the previous work (2.1 m cavity length with 60 cm EDF and 150 cm SMF, 14 μm waist diameter

and 0.8 cm fusion zone length) [19], which benefits the mode-locked of the laser. The pump has the maximum power of 630 mW, and the light of which is integrated into the cavity by a 980/1550 nm wavelength division multiplexer (WDM). The optical coupler (OC) with the output ratio of 20% is able to export the real-time status of the laser. Isolator (ISO) is conducted to avoid reverse transmission of light in the cavity. A polarization controller (PC) is aimed at optimizing intra-cavity birefringence and adjusting polarization states.

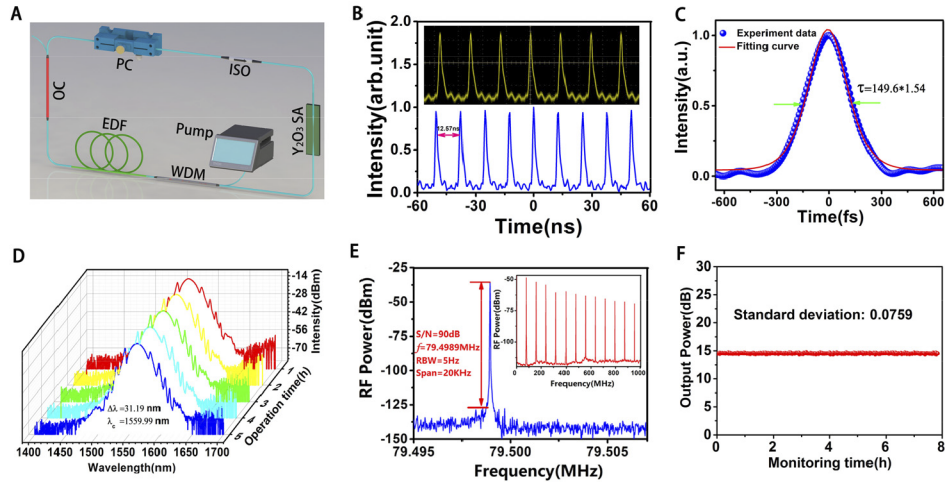


Fig. 3. Construction and results of mode-locked laser based on 5 nm Y_2O_3 . (A) Experimental installation diagram. (B) Mode-locked waveform. (C) Autocorrelation trace. (D) Spectrum. (E) Radio frequency (RF) spectrum. (F) Power jitter.

Three Y_2O_3 samples with different thickness are separately inserted into the laser. Meanwhile, the devices and cavity length remain unchanged during the replacement of different SAs. In the first experiment, the 5 nm Y_2O_3 SA is inserted into the laser. Fine-tuning the polarization state in the cavity after adjusting pump power to an appropriate value, a mode-locked waveform appears on the oscilloscope. The mode-locked threshold is 138 mW. With the increase of pump power, the stable mode-locked waveform is continuously displayed on the oscilloscope. The performance of PMLFL at 630 mW is shown in Fig. 3. The mode-locked pulses show the interval time of 12.57 ns (Fig. 3(B)). From the fitting sech2 profile of experimental data points, the pulse duration (τ) is measured as 149.6 fs (Fig. 3(C)). The spectrum centered at 1559.99 nm with 3-dB bandwidth of 31.19 nm (Fig. 3(D)). Symmetrical sidebands distributed on either side of the spectrum indicate that this is typical soliton mode-locking, and solitons can be separated from Kelly sidebands [36]. The radio frequency (RF) spectrum with 5 Hz resolution and 20 kHz span of mentioned mode-locked system is shown in Fig. 3(E). The signal-to-noise ratio (SNR) and fundamental repetition rate (FRR) are 90 dB and 79.4989 MHz. Considering the large SNR and uniform attenuation trend of frequency multiplication, the mode-locked system is deemed to have good stability. Meanwhile, the corresponding standard deviation of long-term output power is also calculated. The power jitter of the mode-locked laser is 0.0759 dB (Fig. 3(F)). Because of the characteristics of the material and the role of the tapered fiber, SAs with a large modulation depth have a high operating threshold so that it can withstand high pump power. This is beneficial for the signal-to-noise ratio and the stability of the mode-locking. Besides, the tapered fiber can effectively carry out nonlinear control and avoid pulse splitting. Thus, the single pulse output is still maintained at a higher pump power.

Subsequently, the 8 nm Y_2O_3 SA is employed in the same cavity. After fine tuning of PC, a stable mode-locked system is gotten. The FRR is given as 79.6738 MHz (Fig. 4(A)), which

is within reasonable margin of error compared with that of aforementioned laser. The SNR is measured as 87 dB. The τ is measured as 164.4 fs (Fig. 4(B)). At this time, the power jitter of the system within 8 hours is 0.0759 dB (Fig. 4(C)). Finally, the 20 nm- Y_2O_3 SA is inserted between WDM and ISO. Similar mode-locked sequences are also obtained after fine-tuning PC. The FRR of 79.7802 MHz is almost the same as the previous two comparative tests (Fig. 4(D)). The SNR is measured as 82 dB. τ is 176.2 fs (Fig. 4(E)). The power jitter of mode-locked laser based on Y_2O_3 with the thickness of 20 nm is 0.1330 dB (Fig. 4(F)). When we remove the SA inside the fiber laser, there is no mode locking, indicating that the SA is crucial to the mode locking.

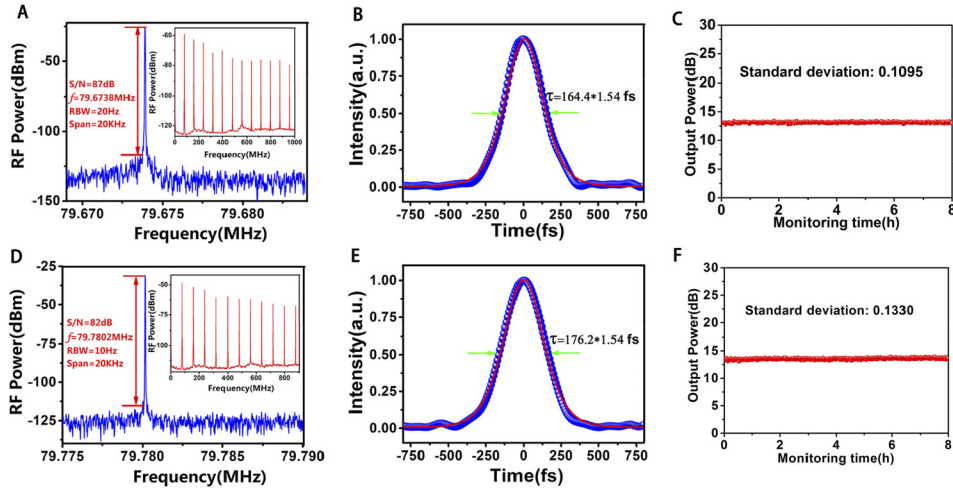


Fig. 4. Experimental results of mode-locked laser based on 8 nm and 20 nm Y_2O_3 . RF spectrum, autocorrelation trace and power jitter of mode-locked laser based on (A)(B)(C)8 nm- and (D)(E)(F)20 nm- Y_2O_3 films.

3. Discussion

A more detailed performance summary of three lasers is presented in Table 1. We find that Y_2O_3 show the strong nonlinearity under three different thicknesses, which indicates that it has a strong ability to modulate light. Furthermore, by comparison, Y_2O_3 with thickness of 5 nm not only shows the maximum modulation depth, but also has advantages in the generation of ultra-short pulses. In addition, the stability of the laser based on 5-nm Y_2O_3 is the best, and the output power of 29 mW is also the largest.

Table 1. Performance summary of three lasers.

Materials	MD ^a	λ (nm)	Rep ^b (MHz)	P ^c (mW)	SNR ^d (dB)	τ (fs)	SD ^e
Y_2O_3 (5nm)	52.4%	1559.99/31.19	79.499	29	90	149.6	0.0759
Y_2O_3 (8nm)	45.3%	1558.5/30.42	79.6738	19.8	87	164.4	0.1095
Y_2O_3 (20nm)	42.43%	1560/29.75	79.7802	23	82	176.2	0.1330

^aModulation depth;

^bRepetition rate;

^cOutput power;

^dSignal-to-noise ratio;

^eStandard deviation

In order to analyze laser performance more comprehensively, the proposed lasers are also compared with some other SA-based lasers in Table 2. It is notable that the structure of microfiber

has great advantages for the nonlinearity of Y_2O_3 SA. As a result, the MD of Y_2O_3 SA is almost the largest in Table 2. Meanwhile, Y_2O_3 also has considerable potential and advantages in the generation of ultra-short pulses. In addition, long term power stability monitoring shows that the system we implemented is relatively stable. Thus, as a SA, the comprehensive performance and potential of Y_2O_3 are impressive, and we look forward to its follow-up research and business development.

Table 2. Output performance comparison of SA-based lasers.

Materials	MD	λ (nm)	τ (fs)	SNR (dB)	P(mW)	Refs.
CNTs	15.8%	1554/41	97	-	3.93	[37]
Graphene	4.8%	1545/48	88	65	1.5	[2]
BP	8.1%	1571.45/2.9	946	>70	-	[38]
Bi_2Se_3	3.9%	1557.5/4.3	660	>55	-	[39]
WS_2	25.48%	1561/57	246	92	18	[40]
MoS_2	35.4%	1568.9/2.6	1280	62	5.1	[41]
$MoSe_2$	5.4%	1557.3/5.4	737	61.9	3.96	[42]
WSe_2	0.3%	1556.7/2	1310	<50	0.45	[43]
Y_2O_3	52.4%	1559.99/31.19	149.6	90	29	This work

4. Conclusion

By magnetron sputtering method, the Y_2O_3 SA with the tapered fiber structure has been successfully prepared. The electronic band structures of Y_2O_3 have been theoretically calculated. In order to prove the optical nonlinearity of Y_2O_3 , it has been employed into the laser cavity as the SA. As a result, the PMLFL based on Y_2O_3 has been realized. Besides, the effect of Y_2O_3 thickness on the performance of lasers has been investigated. Comparison of experimental results have showed that Y_2O_3 with a thickness of 5 nm has been the advantageous than those of thicker materials in achieving PMLFL with short pulse duration, high output power and high stability. This research not only investigates the optical nonlinearity of Y_2O_3 , but also paves the way for further development and research of Y_2O_3 in optics and optoelectronics.

Funding. National Natural Science Foundation of China (11875008, 11975172, 12075034); Fundamental Research Funds for the Central Universities (2019XD-A09-3); Beijing University of Posts and Telecommunications (IPOC2019ZZ01).

Acknowledgements. We thank the Institute of Physics in Chinese Academy of Sciences for characterization of SA.

Disclosures. The authors declare no conflicts of interest.

Data availability. Data underlying the results presented in this paper are not publicly available at this time but may be obtained from the authors upon reasonable request.

References

1. H. Zhang, D. Y. Tang, L. M. Zhao, Q. L. Bao, and K. P. Loh, "Large energy mode locking of an erbium-doped fiber laser with atomic layer graphene," *Opt. Express* **17**(20), 17630–17635 (2009).
2. S. Jaroslaw, P. Iwona, K. Aleksandra, S. Wlodek, and S. Grzegorz, "Sub-90 fs a stretched-pulse mode-locked fiber laser based on a graphene saturable absorber," *Opt. Express* **23**(21), 27503–27508 (2015).
3. P. G. Yan, A. J. Liu, Y. S. Chen, J. Z. Wang, S. C. Ruan, H. Chen, and J. F. Ding, "Passively mode-locked fiber laser by a cell-type WS_2 nanosheets saturable absorber," *Sci. Rep.* **5**(1), 12587 (2015).
4. K. Wu, C. S. Guo, H. Wang, X. Y. Zhang, J. Wang, and J. P. Chen, "All-optical phase shifter and switch near 1550 nm using tungsten disulfide (WS_2) deposited tapered fiber," *Opt. Express* **25**(15), 17639–17649 (2017).
5. Z. Luo, Y. Huang, Z. Min, Y. Li, and J. Weng, "1-, 1.5-, and 2- μ m fiber lasers Q-switched by a broadband few-layer MoS_2 saturable absorber," *J. Lightwave Technol.* **32**(24), 4077–4084 (2014).

6. W. J. Liu, L. H. Pang, H. N. Han, W. L. Tian, H. Chen, M. Lei, P. G. Yan, and Z. Y. Wei, “70-fs mode-locked erbium-doped fiber laser with topological insulator,” *Sci. Rep.* **6**(1), 19997 (2016).
7. J. Sotor, G. Sobon, W. Macherzynski, P. Paletko, K. Grodecki, and K. M. Abramski, “Mode-locking in Er-doped fiber laser based on mechanically exfoliated Sb_2Te_3 saturable absorber,” *Opt. Mater. Express* **4**(1), 1–6 (2014).
8. A. S. Rodin, A. Carvalho, and A. H. C. Neto, “Strain-induced gap modification in black phosphorus,” *Phys. Rev. Lett.* **112**(17), 176801 (2014).
9. Y. H. Xu, Z. T. Wang, Z. N. Guo, H. Huang, Q. L. Xiao, H. Zhang, and X. F. Yu, “Solvochemical synthesis and ultrafast photonics of black phosphorus quantum dots,” *Adv. Opt. Mater.* **4**(8), 1223–1229 (2016).
10. X. T. Jiang, S. X. Liu, W. Y. Liang, S. J. Luo, Z. L. He, Y. Q. Ge, H. D. Wang, R. Cao, F. Zhang, Q. Wen, J. Q. Li, Q. L. Bao, D. Y. Fan, and H. Zhang, “Broadband nonlinear photonics in few-layer MXene $\text{Ti}_3\text{C}_2\text{Tx}$ (T = F, O, or OH),” *Laser Photonics Rev.* **12**(2), 1700229 (2018).
11. J. H. Shim, C. C. Chao, H. Huang, and F. B. Prinz, “Atomic layer deposition of yttria-stabilized zirconia for solid oxide fuel cells,” *Chem. Mater.* **19**(15), 3850–3854 (2007).
12. S. Zhu, X. T. Zu, L. M. Wang, and R. C. Ewing, “Nanodomains of pyrochlore formed by Ti ion implantation in yttria-stabilized zirconia,” *Appl. Phys. Lett.* **80**(23), 4327–4329 (2002).
13. J. Niinistö, M. Putkonen, and L. Niinistö, “Processing of Y_2O_3 thin films by atomic layer deposition from cyclopentadienyl-type compounds and water as precursors,” *Chem. Mater.* **16**(15), 2953–2958 (2004).
14. V. H. Mudavakkat, V. V. Atuchin, V. N. Kruchinin, A. Kayani, and C. V. Ramana, “Structure, morphology and optical properties of nanocrystalline yttrium oxide (Y_2O_3) thin films,” *Opt. Mater.* **34**(5), 893–900 (2012).
15. G. Bonnet, M. Lachkar, J. P. Larpin, and J. C. Colson, “Organometallic chemical vapor deposition of rare earth oxide thin films. Application for steel protection against high temperature oxidation,” *Solid State Ion.* **72**, 344–348 (1994).
16. G. D. Wilk, R. M. Wallace, and J. M. Anthony, “High- κ gate dielectrics: Current status and materials properties considerations,” *J. Appl. Phys.* **89**(10), 5243–5275 (2001).
17. P. Rouffignac, J. S. Park, and R. G. Gordon, “Atomic layer deposition of Y_2O_3 thin films from yttrium tris (N, N’-diisopropylacetamidate) and water,” *Chem. Mater.* **17**(19), 4808–4814 (2005).
18. A. Choudhary, S. Dhingra, B. D’Urso, T. L. Parsonage, K. A. Sloyan, R. W. Eason, and D. P. Shepherd, “Q-switched operation of a pulsed-laser-deposited Yb: Y_2O_3 waveguide using graphene as a saturable absorber,” *Opt. Lett.* **39**(15), 4325–4328 (2014).
19. M. L. Liu, W. J. Liu, X. M. Liu, Y. Y. Ouyang, H. R. Hou, M. Lei, and Z. Y. Wei, “Yttrium oxide as a Q-switcher for the near-infrared erbium-doped fiber laser,” *Nanophotonics* **9**(9), 2887–2894 (2020).
20. J. D. Yin, H. Chen, W. Lu, M. L. Liu, I. L. Li, M. Zhang, W. F. Zhang, J. Z. Wang, Z. H. Xu, P. G. Yan, W. J. Liu, and S. C. Ruan, “Large-area and highly crystalline MoSe_2 for optical modulator,” *Nanotechnology* **28**(48), 484001 (2017).
21. W. J. Liu, M. L. Liu, Y. Y. Ouyang, H. R. Hou, G. L. Ma, M. Lei, and Z. Y. Wei, “Tungsten diselenide for mode-locked erbium-doped fiber lasers with short pulse duration,” *Nanotechnology* **29**(17), 174002 (2018).
22. Z. P. Sun, T. Hasan, F. Torrisi, D. Popa, G. Privitera, F. Q. Wang, F. Bonaccorso, D. M. Basko, and A. C. Ferrari, “Graphene mode-locked ultrafast laser,” *ACS Nano* **4**(2), 803–810 (2010).
23. W. J. Liu, M. L. Liu, J. D. Yin, H. Chen, W. Lu, S. B. Fang, H. Teng, M. Lei, P. G. Yan, and Z. Y. Wei, “Tungsten diselenide for all-fiber lasers with the chemical vapor deposition method,” *Nanoscale* **10**(17), 7971–7977 (2018).
24. J. Q. Zhu, Y. K. Zhu, W. X. Shen, Y. J. Wang, J. C. Han, G. Tian, P. Lei, and B. Dai, “Growth and characterization of yttrium oxide films by reactive magnetron sputtering,” *Thin Solid Films* **519**(15), 4894–4898 (2011).
25. Q. Bao, H. Zhang, Z. Ni, Y. Wang, L. Polavarapu, Z. Shen, Q.-H. Xu, D. Tang, and K. P. Loh, “Monolayer graphene as a saturable absorber in a mode-locked laser,” *Nano Res.* **4**(3), 297–307 (2011).
26. G. Kresse and J. Furthmüller, “Efficient iterative schemes for ab initio total-energy calculations using a plane-wave basis set,” *Phys. Rev. B* **54**(16), 11169–11186 (1996).
27. G. Kresse and D. Joubert, “From ultrasoft pseudopotentials to the projector augmented-wave method,” *Phys. Rev. B* **59**(3), 1758–1775 (1999).
28. J. P. Perdew, K. Burke, and M. Ernzerhof, “Perdew, burke, and ernzerhof reply,” *Phys. Rev. Lett.* **80**(4), 891 (1998).
29. H. J. Monkhorst and J. D. Pack, “Special points for Brillouin-zone integrations,” *Phys. Rev. B* **13**(12), 5188–5192 (1976).
30. J. Heyd, G. E. Scuseria, and M. Ernzerhof, “Hybrid functionals based on a screened Coulomb potential,” *J. Chem. Phys.* **118**(18), 8207–8215 (2003).
31. A. V. Krukau, O. A. Vydrov, A. F. Izmaylov, and G. E. Scuseria, “Influence of the exchange screening parameter on the performance of screened hybrid functionals,” *J. Chem. Phys.* **125**(22), 224106 (2006).
32. J. Tao and M. Batzill, “Adsorption of acetic acid on rutile TiO_2 (110) vs (011)- 2×1 surface,” *Surf. Sci.* **115**, 3434–3442 (2011).
33. H. A. Badehian, H. Salehi, and M. Ghohestani, “First-principles study of elastic, structural, electronic, thermodynamical, and optical properties of Yttria (Y_2O_3) ceramic in cubic phase,” *J. Am. Ceram. Soc.* **96**(6), 1832–1840 (2013).
34. T. T. Song, M. Yang, M. Callsen, Q. Y. Wu, J. Zhou, S. F. Wang, S. J. Wang, and Y. P. Feng, “Graphene stabilized high- κ dielectric Y_2O_3 (111) monolayers and their interfacial properties,” *RSC Adv.* **5**(102), 83588–83593 (2015).
35. J. X. Zheng, G. Ceder, T. Maxisch, W. K. Chim, and W. K. Choi, “Native point defects in yttria and relevance to its use as a high-dielectric-constant gate oxide material: First-principles study,” *Phys. Rev. B* **73**(10), 104101 (2006).

36. Y. T. Wang, S. N. Fu, C. Zhang, X. H. Tang, J. Kong, J. H. Lee, and L. M. Zhao, "Soliton distillation of pulses from a fiber laser," *J. Lightwave Technol.* **39**(8), 2542–2546 (2021).
37. J. Z. Wang, Z. P. Cai, P. Xu, G. G. Du, F. Q. Wang, S. C. Ruan, Z. P. Sun, and H. Tawfique, "Pulse dynamics in carbon nanotube mode-locked fiber lasers near zero cavity dispersion," *Opt. Express* **23**(8), 9947–9958 (2015).
38. Y. Chen, G. B. Jiang, S. Q. Chen, Z. N. Guo, X. F. Yu, C. J. Zhao, H. Zhang, Q. L. Bao, S. C. Wen, D. Y. Tang, and D. Y. Fan, "Mechanically exfoliated black phosphorus as a new saturable absorber for both Q-switching and mode-locking laser operation," *Opt. Express* **23**(10), 12823–12833 (2015).
39. H. Liu, X. W. Zheng, M. Liu, N. Zhao, A. P. Luo, Z. C. Luo, W. C. Xu, H. Zhang, C. J. Zhao, and S. C. Wen, "Femtosecond pulse generation from a topological insulator mode-locked fiber laser," *Opt. Express* **22**(6), 6868–6873 (2014).
40. W. J. Liu, L. H. Pang, H. N. Han, K. Bi, M. Lei, and Z. Y. Wei, "Tungsten disulphide for ultrashort pulse generation in all-fiber lasers," *Nanoscale* **9**(18), 5806–5811 (2017).
41. H. D. Xia, H. P. Li, C. Y. Lan, C. Li, X. X. Zhang, S. J. Zhang, and Y. Liu, "Ultrafast erbium-doped fiber laser mode-locked by a CVD-grown molybdenum disulfide (MoS₂) saturable absorber," *Opt. Express* **22**(14), 17341–17348 (2014).
42. J. Koo, J. Park, J. Lee, Y. M. Jhon, and J. H. Lee, "Femtosecond harmonic mode-locking of a fiber laser at 3.27 GHz using a bulk-like, MoSe₂-based saturable absorber," *Opt. Express* **24**(10), 10575–10589 (2016).
43. D. Mao, X. Y. She, B. B. Du, D. X. Yang, W. D. Zhang, K. Song, X. Q. Cui, B. Q. Jiang, T. Peng, and J. L. Zhao, "Erbium-doped fiber laser passively mode locked with few-layer WSe₂/MoSe₂ nanosheets," *Sci. Rep.* **6**(1), 23583 (2016).